Environmental Research 252 (2024) 118976

Contents lists available at ScienceDirect

Environmental Research

journal homepage: www.elsevier.com/locate/envres

Phosphate adsorption on dried alum sludge: Modeling and application to treatment of dairy effluents

Leila Djekoune [a], Aziz Maaliou [b], Zineb Salem [a], Dalila Ziani [b], Raouf Kamel [a], Abdelkader Ouakouak [c], Omirserik Baigenzhenov [d], Dmitry Olegovich Bokov [e,f], Andrei Ivanets [g], Ahmad Hosseini-Bandegharaei [h,i,j,*]

[a] Faculty of Mechanical and Process Engineering, University of Science and Technology Houari Boumediene, Laboratory of Sciences and Industrial Process Ingeneering, PB 32 El-Alia, Bab - Ezzouar, 16311, Algiers, Algeria
[b] Faculty of Civil Engineering, University of Science and Technology Houari Boumediene, LEGHYD Laboratory, PB 32 El-Alia, Bab - Ezzouar, 16311, Algiers, Algeria
[c] Hydraulic and Civil Engineering Department, University of El Oued, POBox 789, El Oued, 39000, Algeria
[d] Department of Metallurgical Engineering, Satbayev University, Almaty, Kazakhstan
[e] Institute of Pharmacy Named After A.P. Nelyubin, Sechenov First Moscow State Medical University, 8 Trubetskaya St., bldg. 2, Moscow, 119991, Russian Federation
[f] Laboratory of Food Chemistry, Federal Research Center of Nutrition, Biotechnology and Food Safety, 2/14 Ustyinsky pr., Moscow, 109240, Russian Federation
[g] Institute of General and Inorganic Chemistry of the National Academy of Sciences of Belarus, 9/1, Surganova st., 220072, Minsk, Belarus
[h] Faculty of Chemistry, Semnan University, Semnan, Iran
[i] Department of Sustainable Engineering, Saveetha School of Engineering, SIMATS, Chennai, 602105, Tamil Nadu, India
[j] Centre of Research Impact and Outcome, Chitkara University, Rajpura, 140401, Punjab, India

ARTICLE INFO

Keywords:
Alum sludge
Adsorption
Phosphates
Kinetics
Dairy effluent

ABSTRACT

This study evaluates Alum sludge from drinking water treatment plants for the efficient and cost-effective removal of phosphates from aqueous solutions. Extensive characterization and batch experiments have established that optimal phosphate removal was achieved with a sludge dosage of 20 g L^{-1} (at an initial phosphate concentration of 100 mg L^{-1}), a pH of 5, a temperature of 23 °C, and a stirring speed of 200 rpm. These conditions significantly reduced phosphate levels, ensuring compliance with legal discharge limits. The Langmuir isotherm, pseudo-second-order kinetic and intraparticle diffusion models best described the adsorption process, highlighting the spontaneous and endothermic nature of the phenomenon. The sludge effectively reduced phosphate concentrations to acceptable levels when applied to dairy effluents. This study underscores the potential of Alum sludge as a viable solution for phosphate management in environmental cleanup efforts.

1. Introduction

Currently, the intensification of agricultural activities, including soil fertility, poultry farming and some food industries generate high levels of phosphorus in waters (Adhikari et al., 2016). Phosphorus is one of the main nutrients causing eutrophication of aquatic environment above 0.1 mg P L^{-1} (Harrison, 2001). But it is also the limiting factor to this phenomenon if removed. Biological procedures and physico-chemical treatments are widely used for phosphorus uptake (Adhikari et al., 2016; Li et al., 2019). Due to its convenience, reliability and cost-effectiveness, sorption technology is widely used (Li et al., 2015, 2019; Zhu et al., 2020; Moreira et al., 2017). Low cost adsorbent such as fly ashes (Lu et al., 2009), red muds (Yue et al., 2013), natural sorbents (Moharami and Jalali), activated carbon (Sirajo and Zaini, 2023), treated aluminium waste-filings (Qasemi et al., 2018), and iron–related chemicals (Lǔ et al., 2013) have used for phosphate removal. These sorbent materials are mainly made up of natural minerals, industrial by products, agricultural waste solids and synthetic substances (Makris et al., 2006). Therefore, valorising mineral waste such as sludge from plants producing drinking water would be most economical.

Some treatments use coagulation-flocculation method with aluminum sulfate as one of coagulants. The ferruginous nature and hardness of waters to be treated results in a mixture of aluminum, iron and calcium oxides. Their presence is important because the oxides of such elements are helpful in phosphate removing by sorption, ion-exchange or precipitation methods (Yang et al., 2006; Tang et al., 2006).

* Corresponding author. Faculty of Chemistry, Semnan University, Semnan, Iran.
E-mail address: ahoseinib@semnan.ac.ir (A. Hosseini-Bandegharaei).

https://doi.org/10.1016/j.envres.2024.118976
Received 2 October 2023; Received in revised form 16 April 2024; Accepted 19 April 2024
Available online 4 May 2024
0013-9351/© 2024 Elsevier Inc. All rights reserved.

Several research assessments have reported on the plausible exploitation of Alum sludges as a sorbent for pollutant removal from wastewater. It can used to remove heavy metal contaminants like Cd, Cr, Ni and Pb (Abo-El-Enein et al., 2017; Siswoyo et al., 2014; Jeon et al., 2018), as Jeon et al. (2018) have mentioned (Jeon et al., 2018). In addition, it has been exploited for the removal of other pollutants like fluoride (Sujana et al., 1998), phenolic compounds (Fragoso and Duarte, 2012) and textile dye removal (Chu, 2001). Researchers consider alum sludge one of the principal sorbents for phosphorus (Adhikari et al., 2016; Babatunde et al., 2010; Piaskowski, 2013). Since phosphate chemical species (H_3PO_4, $H_2PO_4^-$, $HPO_4^{2-}$and PO_4^{3-}) vary with the solution Ph, phosphate sorption is a complicated process.

This study focuses on the removal of phosphate from aqueous solutions using cost-effective sorbents such as Alum sludges derived from drinking water treatment plants. The alum sludge used in this study was derived from a sedimentation process at a water treatment plant in Reguig-Kaddour (west of Algiers). We approached the evaluation of this material as a potential sorbent from two perspectives. Firstly, its widespread availability in significant quantities due to its utility, and secondly, its potential for repurposing in wastewater treatment as part of waste management strategies (Djekoune et al., 2022). The novelty of this research lies in its comprehensive assessment of Alum sludge as a sorbent for phosphate removal, taking into account its abundance and reusability in wastewater treatment processes. Furthermore, we demonstrated the practical applicability of Alum sludge by successfully treating real industrial effluents, showcasing its efficacy in meeting regulatory standards for phosphate discharge. For this purpose, first, we exploited XRF (X-ray fluorescence), FTIR spectrometer, SEM (scanning electron microscope), XRD (X-ray diffraction), and BET analyses to study the sorbent. Then, we studied the influence of several physical and chemical parameters in batch adsorption experiments. Also, we investigated sorption kinetics, isotherms and thermodynamic aspects thouroughly. Finally, we attentively assessed this material as a sorbent for a dairy industrial effluent. Overall, this study contributes to advancing sustainable solutions for phosphate remediation, leveraging Alum sludge as a valuable resource in environmental and industrial contexts.

2. Materials and methods

The alum sludges used in the experiments was derived from a sedimentation process at a water treatment plant in Reguig-Kaddour (west of Algiers). We subjected the sludges to a 24-h oven-heating period at 105 °C, followed by cooling to ambient temperature. Afterward, we ground the dried sludges and sieved them to a particle size of 250 μm.

Leaching tests, which are crucial for residue management monitoring, allowed us to study the sludge behavior in water's presence and predict the potential release of pollutants. We performed the leaching test according to the standard X 31–210. We detected the pH at the point of zero charge (pH_{ZPC}) by measuring the equilibrated pHs of solutions containing a salt and adjusted to various values.

Using X-ray fluorescence (XRF), we defined the physio-chemical compositions of the alum sludge. We measured the specific surface area (S_{BET}), total pore volume (V_{Total}), and total pore size with N_2 absorption-desorption isotherms using the Brunauer–Emmett–Teller (BET) procedure. We recorded FT-IR spectra of alum sludge using a KBr Alpha Bruker FT-IR spectrometer in the span of 400–4000 cm^{-1}. We inspected the morphologies of alum sludge particles by Scanning Electron Microscopy using an XL30 ESEM at an accelerating voltage of 20 kV equipped with energy dispersive spectroscopy (EDS). We grasped the structural features of alum sludge by X-ray diffraction (XRD) using an XPERT-PR diffractometer, at 45.0 kV and 40.0 mA, with CuKα radiation (λ = 1.5406 Å) at a scanning speed of 0.01°/s.

The stock solutions of phosphate at 1g L^{-1} were prepared by diluting weighed amounts of KH_2PO_4 in deionized water. By doing necessary dilutions, we attained desired concentrations. We adopted batch tests to follow the uptake kinetics of phosphates on alum sludge. We conducted the experiments in flasks (Erlenmeyers) on temperature set stirrers under the following conditions: adsorbent dosage 10–120 g L^{-1}, initial phosphate level 25–500 mg L^{-1}, temperature 15–75 °C, stirring rates 50–600 rpm, and initial pH solution 3–12. We brought the solution pH to prespecified values by adding HCl (0.1 mol L^{-1}) or NaOH (0.1 mol L^{-1}) and monitored it with a pH-meter (Hanna HI-8224).

We continuously agitated the mixtures to attain equilibrium. Afterward, we subjected each suspension to isolation of sludge from solution by centrifugation at 4000 rpm for 5.0 min, and we inspected the supernatants by Shimadzu UV-1800 spectrophotometer at λ = 700 nm using the molybdenum-blue ascorbic acid method. We conducted duplicated measurements on every sample and exploited the averaged result.

We computed the adsorption capacity at 't' time (q_t; mg g^{-1}) and equilibrium (q_e; mg g^{-1}) from equations (1) and (2):

$$q_t = \frac{(C_0 - C_t)}{m} \times V \quad (1)$$

$$q_e = \frac{(C_0 - C_e)}{m} \times V \quad (2)$$

The phosphate removal rate (removal efficiency; %) was computed employing equation (3):

$$RE\% = \frac{(C_0 - C_t)}{C_0} \times 100 \quad (3)$$

where C_0, C_t and C_e (mg L^{-1}) are, respectively, initial levels, concentrations at 't' times and levels at equilibrium, m (g) sorbent weights, and V (L) is solution volumes.

3. Results and discussion

3.1. Alum sludge characterizations

3.1.1. Leaching tests

The outcomes of the leaching tests were reported in Table 1. The concentrations of the analyzed parameters were very low compared to the standard norms. The concentration of Al^{3+} was 0.075 mg L^{-1}, below the recommended maximum concentration of 5 mg L^{-1} for trace metals in irrigation water, according to FAO guidelines. The leaching tests indicate that this material poses no potential pollutant risks.

3.1.2. Physico-chemical composition of alum sludge and BET analysis

Features of sludges are greatly variable and in tandem with both the chemical composition of coagulants and the types of raw waters subjected to treatment (Sotero-Santos et al., 2005).

We present the physical parameters, chemical composition, and BET analysis in Table 2, demonstrating that Alum sludge has an alkaline property (pH = 8) and a high humidity level. The BOD5 amount indicates low organic matter of the sludge, which reveals its non-fermentability and stability.

Table 2 shows that silica and aluminium are the major components of Alum sludge, comprising approximately 42.0% SiO_2 and 19.73% Al_2O_3, respectively. The other dominant chemical components are CaO and

Table 1
Chemical parameters of raw alum sludge after leaching tests.

Parameters	Value
pH	7.5
Conductivity (μs cm^{-1})	900
Sulfate (mgL^{-1})	416.4
Chloride(mgL^{-1})	103
Aluminum(mgL^{-1})	0.075
Phosphate(mgL^{-1})	0.307
Organic matter (mgL^{-1})	39.1

Table 2
Properties, chemical composition and BET analysis of Alum sludge.

Physiochemical Properties	
pH	8.15
Moisture (%)	90.02
[a]SM (%)	9.98
Porosity (%)	68–69
BOD_5(mg. O_2 L^{-1})	16.37
Chemical composition (%)	
SiO_2	42.09
Al_2O_3	19.73
CaO	08.21
Fe_2O_3	05.57
K_2O	01.74
MgO	01.34
ZnO	0.66
TiO_2	0.59
Na_2O	0.52
Sulfate as SO_3	0.34
Mn_2O	0.06
BaO	0.03
SrO	0.03
[b]LOI	19.78
BET analysis	
S_{BET}(m^2/g)	29.86
$S_{Micropore}$(m^2/g)	1.6699
$S_{External}$(m^2/g)	28.1903
V_{Total}(m^3/g)	0.059
$V_{Micropore}$(m^3/g)	0.0004
$V_{Mesopore}$ (%)	99.32
Pore diameter nm	7.86

[a] SM: Solid matter.
[b] LOI: Loss on ignition at 1000 °C.

Fe_2O_3, with mass percentages of 8.21 and 5.57, respectively. Using aluminium sulfate as a coagulant in water treatment plants may justify the presence of these elements. The composition of water can also be the source of these elements as it contains suspended materials like sand and clay particles. In addition, Loss in Ignition (LOI) shows that the alum sludge includes some organic matter (19.78% by mass).

The specific surface area of alum sludge (S_{BET}) is 29.86 m^2 g^{-1}, and 7.86 nm is the average diameter of its pores. The outcomes vouchsafe that the tested substance structure is predominantly mesoporous ($V_{mesopore}$ = 99.32%), and its total pore volume is almost low (V_{Total} = 0.059 cm^3 g^{-1}).

The findings are similar to those of (Yang et al., 2008), who investigated the impact of ageing on both structural properties and phosphate sorption amount of dewatered alum sludge.

3.1.3. FTIR spectrum of alum sludge

Fig. 1 displays the FTIR spectrum of alum sludge. The widened triplets existing at 3737.11 cm^{-1}, 3622 cm^{-1}, and 3465.5 cm^{-1} are assignable to stretching vibrations of the OH functional moiety of water. The bond present at 1429.6 cm^{-1} with a lower intensity demonstrates the existence of CO_3^{2-} of Calcite. An intense peak at 1033 cm^{-1} indicated the silicate structures' Si–O vibration peak. The remaining peaks betwixt 875.6 cm^{-1} and 472.3 cm^{-1} are assignable to Quartz impurities and Si–O, Si–O–Si, OH stretching vibrations, which are linked to Al(III), Fe (III) and Mg(II) ions.

3.1.4. SEM of alum sludge and their EDS

Fig. 2(a) displays the SEM micrograph of the Alum sludge, revealing grey beads with irregular shapes. Furthermore, the EDS results in Fig. 2 (b) corroborate the fluorescence data.

3.1.5. X-ray diffraction

Researchers universally employ X-ray diffraction to identify crystallized products' nature and structural properties. The XRD pattern of Alum sludge, displayed in Fig. 3, reveals the coexistence of amorphous and crystallized phases, including clay minerals such as Illite and Kaolinite, along with other mineral phases.

3.1.6. pHzpc (pH of zero-point charge) of alum sludge

The zero point of charge (pHzpc) of Alum sludge was determined to be 7.85, as shown in Fig. 4. The surface of Alum sludge becomes positively charged at pH values below the pHzpc, enhancing the sorption of anionic contaminants. In contrast, the adsorption of cationic contaminants is favourable at pH values above the pHzpc. Published works report that Alum sludge's zero point of charge varies between 5.5 and 6.9.

3.2. Parametric evaluation of phosphate sorption on alum sludge

3.2.1. Influence of contact duration

Fig. 5 demonstrates the influence of contact duration on phosphate removal. We can divide the phosphate uptake process into three stages. In the initial 5 min, the fast first stage occurs as phosphate ions attach to available sites on the sorbent's surface, achieving a sorption capacity of 76%. The adsorption rate decreases over the next 55 min as fewer sites remain available. The process reaches equilibrium in the third stage at

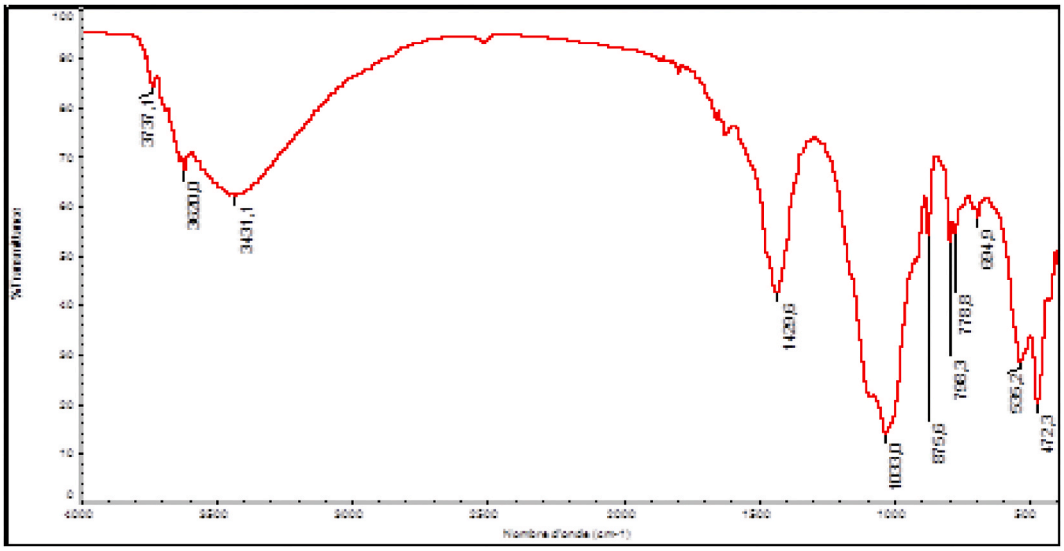


Fig. 1. FTIR spectrum of Alum sludge.

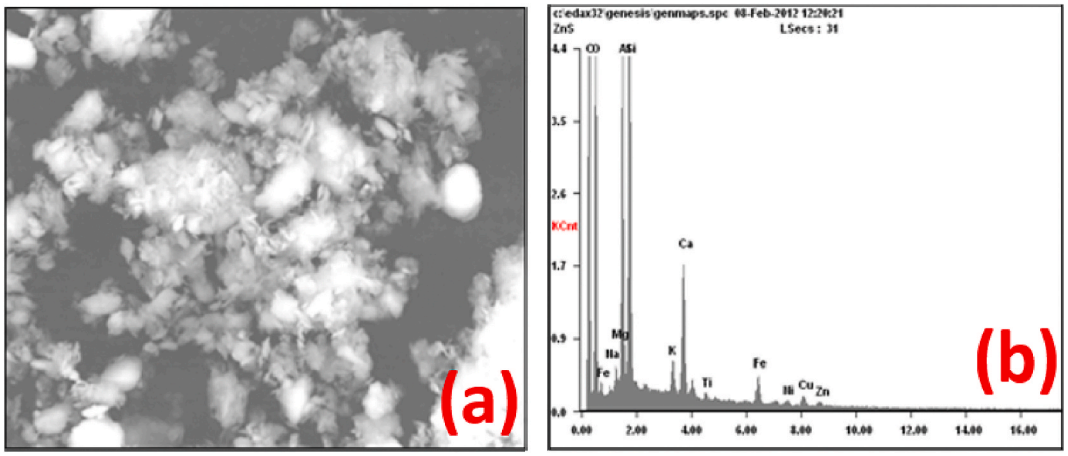


Fig. 2. SEM micrograph(a) and EDS (b) of Alum sludge.

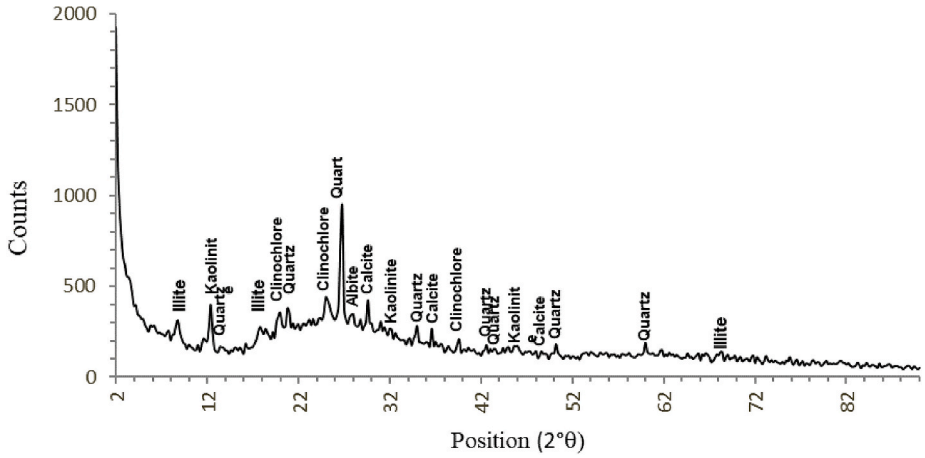


Fig. 3. X-Ray diffraction pattern of Alum sludge.

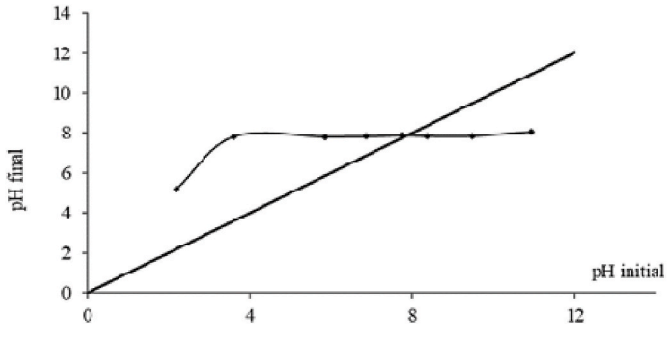


Fig. 4. Zero point charge (pHzpc) of Alum sludge.

60 min, and the sorption capacity remains unchanged.

Table 3 compares the optimal contact times required to reach equilibrium on different materials. We observed a phenomenon in our study that matches those reported in other studies. The contact times range from 5 min to 7 days, depending on the materials.

To inspect the effects of other parameters, the contact time was fixed at 60 min.

3.2.2. *Influence of initial pH*

The phosphate uptake by alum sludge as a pH function was studied. Fig. 6 shows that the sorption capacity of alum sludge increased when the pH rose from 3.0 to 5.0, and then it decreased to 21.6% at pH 12.

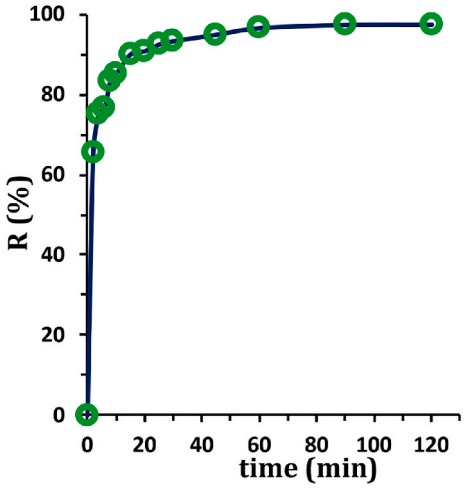


Fig. 5. Influence of contact duration on phosphate removal. (C_0 = 50 mg PL^{-1}, Cs = 20 g L^{-1}, pH_i = 4.35, T = 23 °C, N = 200 rpm).

Phosphate sorption is most favourable at acidic pHs, reaching maximal uptake at pH 5.

This trend can be explained by considering the outcomes of pHzpc and the phosphate speciation, which varies with the solution's pH values. At pH ≤ 3, H_3PO_4 is the predominant phosphate species, loosely

Table 3
Results obtained for adsorption of phosphate onto different materials.

Material	Solution pH	Contact time	Reference
Dewatered alum sludge	4.3	48h	Yang et al. (2008)
Modified bentonite	5.0	2h	Tang et al. (2006)
Red mud	5.0	7h	Zhao et al. (2012a)
Modified fly ash	6.0	60 min	Xu et al. (2012a)
Sintered bottom slag/sewage sludge	6.0	–	Ge et al. (2013a)
Dried Alum sludge	4.3	60 min	Current study

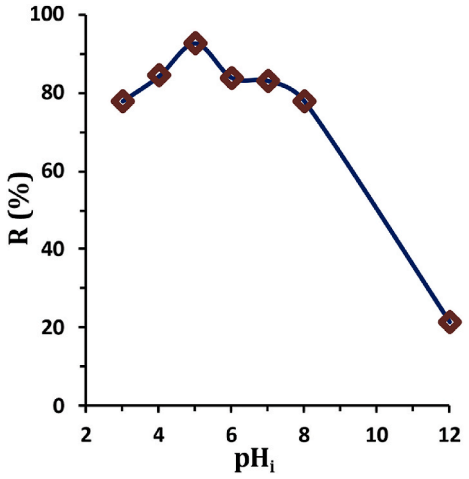


Fig. 6. pH effect on phosphate removal by Alum sludge. (C s = 20 g L^{-1}, C_0 = 100 mg L^{-1}, T = 23 °C, N = 200 rpm and tc = 60 min).

attached to the sorbent sites. However, as the pH increases from 3 to 7, $H_2PO_4^-$ becomes the dominant species (Zhang et al., 2010a; Khitous et al., 2016a). Anion exchange between $H_2PO_4^-$ and OH^- occurs readily, leading to high phosphate removal. At pH ≤ pHzpc, the surface of the Alum sludge carries a positive charge, creating an attractive electrostatic force between the phosphate species and the surface of the Alum sludge. Thus, both anion exchange and electrostatic attraction mechanisms effectively contribute to the uptake of phosphate ions (Khitous et al., 2016a).

As the pH rises above the pHzpc, phosphate removal decreases. The surface of the Alum sludge becomes negatively charged, and HPO_4^{2-} ions emerge as the principal species. The electrostatic repulsion between the sorbent's highly negatively charged surface sites and the anions hinders sorption.

Several other studies have reported similar results (Zhang et al., 2010a, 2010b; Khitous et al., 2016a, 2016b; Zhao et al., 2012b; Xu et al., 2012b; Ye et al., 2006; Mangwandi et al., 2014). The data tabulated in Table 3 also shows that an acidic solution pH is suitable for the process of adsorption from aqueous solutions.

3.2.3. Effect of adsorbent dose

Fig. 7 illustrates that the phosphate removal rapidly increased from 45.4% to 96.7% as we raised the sorbent dosage from 10 to 20 g L^{-1}. We attribute this increase to the abundant availability of phosphate sites at higher sorbent dosages. However, increasing the sorbent dosage from 20 to 120 g L^{-1} does not change phosphate uptake, indicating an optimal dosage for maximal phosphate removal at 20 g L^{-1}. Xu et al. (2012) reported a similar optimal dose using modified fly ash (Xu et al., 2012b). Using thermally treated waste iron oxide material Chen et al. (2013) determined the optimum adsorbent amount to be 10 g L^{-1} (Chen et al., 2013), while using oven-dried alum sludge, Mohammed and Rashid (2012) identified a larger optimal dose of 50 g L^{-1} (Mohammed and Rashid, 2012).

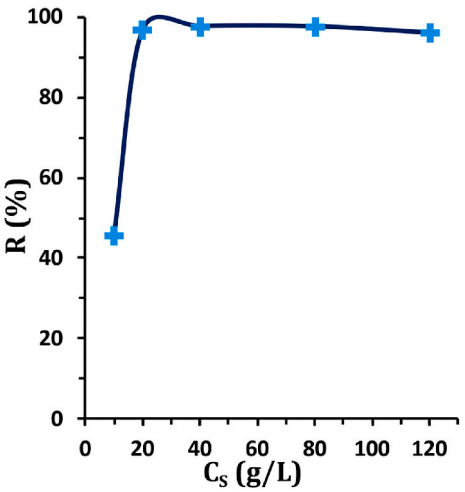


Fig. 7. Adsorbent dose effect on the phosphate removal. (C_0 = 50 mg PL^{-1}, pH_i = 5, T = 23 °C, N = 200 rpm and tc = 60 min).

3.2.4. Influence of initial phosphate level

Fig. 8 shows phosphate removal decreases from 99.0 to 42.7% as the initial concentration increases from 25 to 500 mg L^{-1}. The phosphate removal efficiency decreased with an increase in the initial phosphate concentration.

At the lower pollutant concentrations, enough high energy adsorption sites are available, resulting in the high adsorption capacity, while with increasing initial phosphate concentrations, the high energy adsorption sites became saturated and more pollutant left unadsorbed in the solution due to the saturation of binding sites. This reduction occurs because, for a set amount of sorbent in the aqueous phase, only a limited number of active sites are available for adsorbing a constrained amount of sorbate; these sites become insufficient at higher concentrations. Using oven-dried alum sludge, Mohammed and Rashid (2012) determined the optimal concentration to be 5 mg L^{-1} (Mohammed and Rashid, 2012), while Tang et al. (2006) found it to be 30 mg L^{-1} on modified bentonite (Tang et al., 2006).

Several researchers have studied the effect of initial concentration, finding that the optimum concentrations depend on the properties of the materials studied (Tang et al., 2006; Chu, 2001).

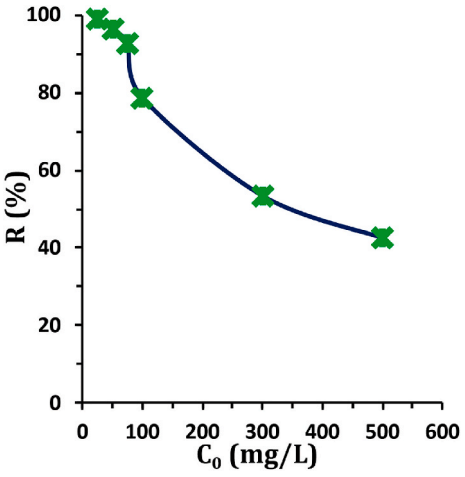


Fig. 8. Initial phosphate concentration effect on the sorption capacity of Alum sludge. (C s = 20 g L^{-1}, pH_i = 5, T = 23 °C, N = 200 rpm and t = 60 min).

3.2.5. Effect of stirring speed

Fig. 9 displays the influence of agitation on phosphate uptake. It was found that the amount of phosphate increased with increase in agitation when agitation speed increased from 100 to 200 rpm because increase in agitation speed reduces the formation of film boundary layer around the adsorbent surface and thus increasing the adsorption capacity of the adsorbent (Nassef, 2012). However, beyond 200 rpm, phosphate removal decreases due to the vortex phenomenon.

The optimum stirring speeds for phosphate adsorption by various materials, as determined by different authors, rang between 100 and 250 rpm (Zhao et al., 2012b; Ge et al., 2013b; Yeddou Mezenner and Bensmaili, 2009; Xiong et al., 2011). For dried Alum sludge studied in the present work, the optimum speed was found to be 200 rpm.

3.2.6. Effect of temperature

Fig. 10 shows phosphate removal rapidly increases with temperature from 15 to 23 °C and then levels off, achieving similar results at higher temperatures (91–97%). Beyond this point, temperature no longer significantly affects the process, making 23 °C the optimal temperature. Similar results were found by Zhao et al. (2012b) with red mud at 27 °C and by Xu et al. (2012) with modified fly ash at 30 °C (Xu et al., 2012b). These studies support our findings. Higher temperatures provide sorbate molecules with more kinetic energy, enhancing their transport within the sorbent's pores. Additionally, as noted by (Nthumbi et al., 2012), the increase in sorption rate with rising temperature is likely due to the breakage of some internal bonds near the sorption sites. This phenomenon might also result from the enlargement of the particles' pore sizes, activation of the sorbent surface, or a catalytic effect of temperature on reaction dynamics.

3.3. Phosphate sorption isotherm

Fig. 11 demonstrates the sorption isotherms of phosphate on Alum sludge. We characterize the isothermal data by a typical L curve isotherm (Ge et al., 2013b), indicating that Alum sludge has a strong sorption affinity toward phosphate in solutions. This finding suggests that the sorption efficiency for phosphate under low initial concentrations was approximately 99%. We used three isothermal models — Langmuir, Freundlich, and Dubinin-Radushkevich — as detailed in equations (4) to (6) (Nthumbi et al., 2012; Zhang et al., 2007; Langmuir, 1916; Foo and Hameed, 2010; Peiravi-Rivash et al., 2023), to fit the data obtained from the experimental tests (Table 4).

Where q_e is phosphate amounts sorbed per sorbent unit (mg. g^{-1}), and C_e is the equilibrium level in solutions (mg. L^{-1}). The remaining factors are constants and characteristics of various isotherms and are measurable by regression of experimental outcomes.

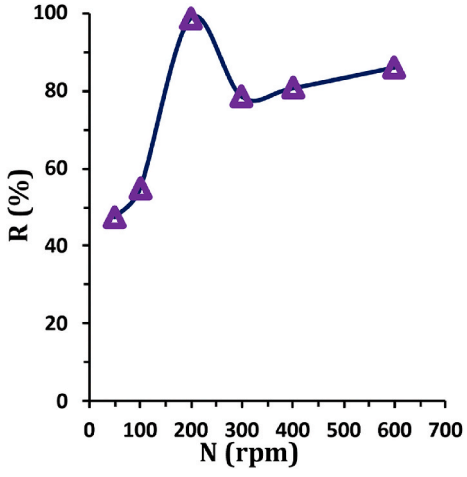


Fig. 9. Stirring speed effect on phosphate removal on Alum sludge. (Cs = 20 g L^{-1}, C_0 = 100 mg PL^{-1}, T = 23 °C, pH = 5 and t = 60 min).

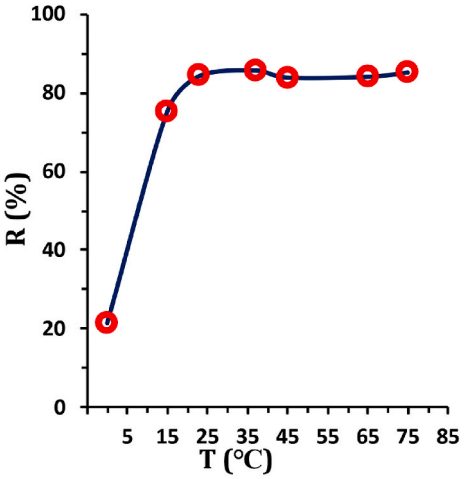


Fig. 10. Temperature effect on the phosphate removal on Alum sludge. (C s = 20 g L^{-1}, C_0 = 100 mg L^{-1}, N = 200 rpm, pH = 5 and t = 60 min).

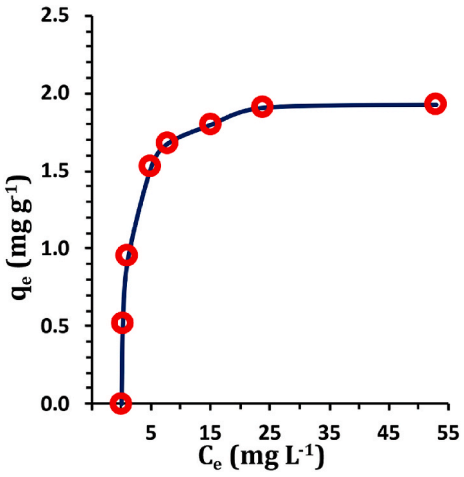


Fig. 11. Phosphate adsorption isotherm on Alum sludge. (C_S = 20 g L^{-1}, N = 200 rpm, initial pH = 5, T = 23 °C et t = 60 min).

Table 4
Mathematical relations of isothermal models.

Isotherms	Non-linear equations	Linear expressions	plots	no (Eq)
Langmuir	$q_e = \frac{q_m K_L C_e}{1 + K_L C_e}$	$\frac{C_e}{q_e} = \frac{1}{q_m} C_e + \frac{1}{K_L q_m}$	$\frac{C_e}{q_e}$ vs. C_e	(4)
Freundlich	$q_e = K_F C_e^{1/n}$	$\ln q_e = \ln K_F + \frac{1}{n} \ln C_e$	$\ln q_e$ vs. $\ln C_e$	(5)
Dubinin-Radushkevich	$q_e = (q_m) exp(-K_d \varepsilon^2)$	$\ln q_e = \ln q_s - K_d \varepsilon^2$	$\ln q_e$ vs. ε^2	(6)

Four error functions which have been presented in equations (7)–(10) are usually recruited for error analyses and quantitative comparison of goodness-of-fits of various sorption isotherms with experimental outcomes.

- SSE (sum of squares of errors) (Kundu and Gupta, 2006):

$$SSE = \sum_{i=1}^{n} \left(q_{e,cal} - q_{e,\exp}\right)_i^2 \quad (7)$$

- SAE (sum of absolute errors) (Kundu and Gupta, 2006):

$$SAE = \sum \left|q_{e,cal} - q_{e,\exp}\right|_i \quad (8)$$

- HYBRID (hybrid fractional error function) (Kundu and Gupta, 2006):

$$HYBRID = \frac{100}{n-p} \sum_{i=1}^{n} \left[\frac{\left(q_{e,\exp} - q_{e,cal}\right)^2}{q_{e,\exp}}\right]_i \quad (9)$$

- NPSD (normalized percentage standard deviation) (Sun and Yang, 2003):

$$NPSD = 100\sqrt{\frac{1}{n-1} \sum_{i=1}^{n} \left(\frac{q_{e,\exp} - q_{e,cal}}{q_{e,\exp}}\right)_i^2} \quad (10)$$

Where $q_{e,exp}$ and $q_{e,\ cal}$ were experimental amounts and computed amounts by sorption isotherm, respectively, p and n refer to the numbers of isotherm parameters and data points, respectively.

We summarize the estimated model parameters, the correlation coefficient R^2, and the error analyses using four error functions for various isotherms in Table 5. Fig. 12 also displays the fitted curves of the sensed isothermal equations.

Similarly, we can compare the correlation coefficients R^2 and four statistical functions for various isotherms, as demonstrated in Fig. 13. The results from the phosphate uptake experiments on Alum sludge show high compatibility with the Langmuir isotherm, suggesting monolayer sorption onto a surface with a finite number of equivalent sites.

A comparison of the maximal phosphate sorption capacity of Alum sludge with other sorbents was performed with some adsorbents like modified red mud, dewatered Alum sludge, slag microspheres, granular red mud, etc. (Yue et al., 2013; Yang et al., 2008; Yousif et al., 2012; Lee et al., 2012). The maximum quantities of phosphates adsorbed on such materials range from 0.558 to 10.95 mg g^{-1}. Comparing our results with previous studies is challenging because they generally occurred under different experimental conditions.

Table 5
Isothermal factors with errors analyses for phosphate sorption on Alum sludge.

Equations	Parameter	magnitude
Langmuir $q_e = \frac{q_m K_L C_e}{1 + K_L C_e}$	q_m (mg.g^{-1})	1.974
	K_L (L.mg^{-1})	0.858
	R^2	0.999
	R_L	0.013
	SSE	0.03
	SSE	0.043
	SAE	0.382
	HYBRID	1.173
	NPSD	0.135
Freundlich $ln\ q_e = K_F C_e^{1/n}$	n_F	0.252
	k_F	0.873
	R^2	0.963
	SSE	0.309
	SAE	1.117
	HYBRID	3.043
	NPSD	0.133
Dubinin-Radushkevich $q_e = (q_m)exp(-K_d\varepsilon^2)$	E (kJ mol^{-1})	3.664
	R^2	0.858
	SSE	0.364
	SAE	1.270
	HYBRID	4.942
	NPSD	0.195

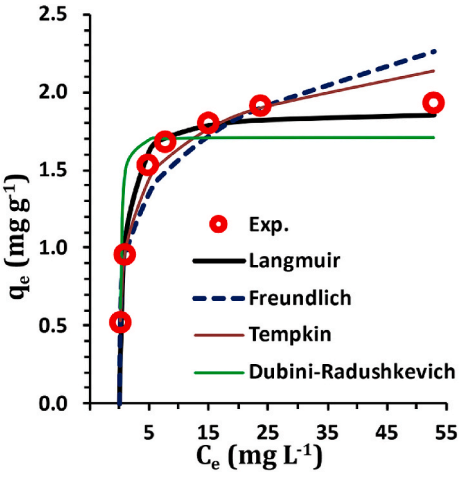


Fig. 12. Plots of determined and computed outcomes of phosphate sorption on Alum sludge. (Cs = 20 g L^{-1}; T = 23 °C; pH = 5; N = 200 rpm).

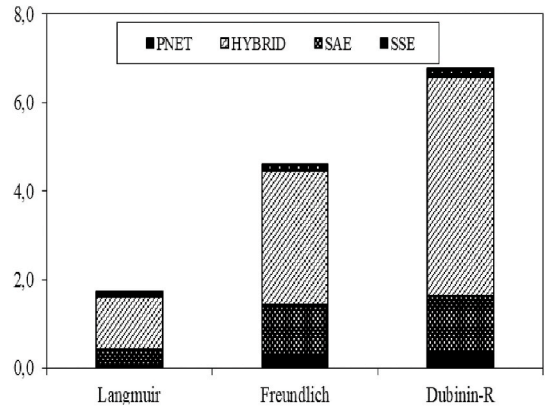


Fig. 13. Comparing of isothermal models in the data fittness from errors analyses.

3.4. Sorption kinetics

In order to explain the mechanism involved in sorption process, three kinetic models were fitted with the phosphate sorption kinetic results: pseudo-first order, pseudo-second order, and intraparticle diffusion model, which were described below in Eqs (11)–(13) respectively:

$$\ln(q_e - q_t) = \ln(q_e) - k_1.t \quad (11)$$

$$\frac{t}{q_t} = \frac{1}{k_2 q_e^2} + \frac{t}{q_e} \quad (12)$$

$$q_t = k_i t^{1/2} + C \quad (13)$$

where q_e and q_t represent the phosphate capacities uptaken by Alum sludge (mg g^{-1}) at equilibrium and at time 't', respectively, k_1 (min^{-1}) and k_2 (g mg^{-1} min^{-1}) are the rate constants of the pseudo-first-order and pseudo-second-order equations. In contrast, k_i (mg g^{-1} $min^{-0.5}$) is the intraparticle diffusion rate constant, and C is the intercept. The kinetic parameters are determined from the slope and intercept of the linear plots of the model equations, as depicted in Fig. 14(a–c). We summarized the obtained outcomes in Table 6.

Based on correlation coefficients R^2 and phosphate capacity at equilibrium capacities computed by the tested equations, and compared with the experimental ones, it was concluded that the pseudo-second-order equation provided a high fitness with the phosphate uptake

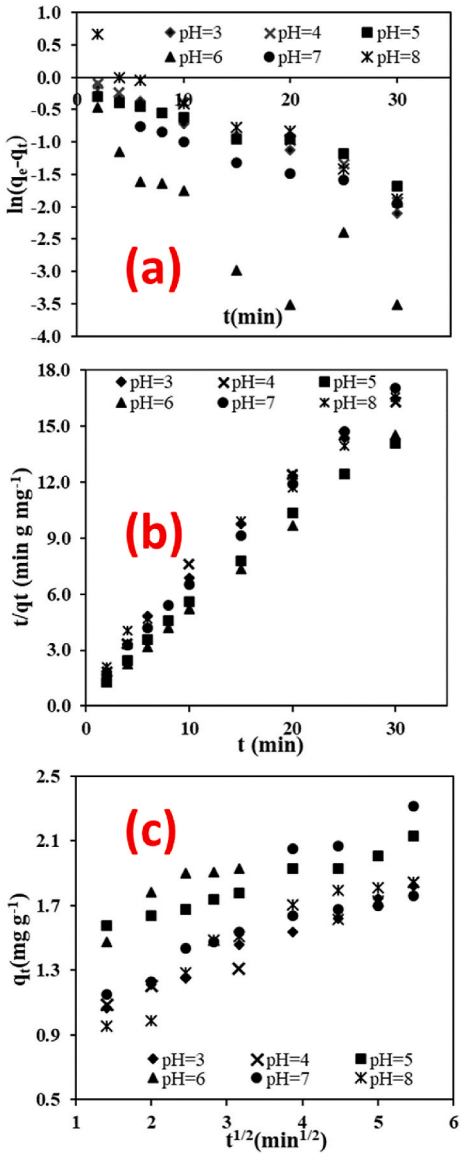


Fig. 14. Kinetics plot regression for phosphate adsorption onto Alum sludge: (a) pseudo-first-order model, (b) pseudo-second-order model, and (c) intra-particle diffusion models.

results.

The calculated kinetics parameters k_2 increase as pH tends towards acidity (Table 6). Other studies have confirmed that phosphate sorption on mineral sorbents follows the pseudo-second-order kinetic model (Cheng et al., 2010; Yan et al., 2014). The second order model postulates that sorption processes are of pseudo-second-order and rate-limiting stage is interaction of adsorbate with the adsorbents sites. The involved mechanisms might be electrostatic interactions or ion exchange betwixt the sorbent and sorbate (Khitous et al., 2016b).

Fig. 14(c) depicts plots of qt versus $t^{1/2}$, divided into two phases. Table 6 shows that the correlation coefficients of each fitted plot are greater than 0.90, indicating that the intraparticle diffusion model provides a good simulation within the corresponding sorption period. This implies that intraparticle diffusion contributes to the uptake process. However, intraparticle diffusion is not the sole rate-limiting step, as none of the phase plots passes through the origin (Fig. 14(c)) (Bulut et al., 2008; Hu et al., 2011).

The first sharper region represents a gradual sorption stage attributed to the anion-exchange reaction between phosphate and Alum sludge. The second region denotes the equilibrium stage, where phosphate uptake begins to slow down.

Table 6
Kinetics factors for phosphate uptake exploiting Alum sludge at various pH_s.

Parameters of kinetic models	pH_i of phosphate solution					
	3.00	4.00	5.00	6.00	7.00	8.00
q_{exp} (mgg^{-1})	1.94	1.99	2.32	2.10	1.91	1.95
Pseudo first-order kinetic model						
q_e (mgg^{-1})	0.98	0.91	3.30	2.37	1.91	1.65
k_1 (min^{-1})	0.065	0.061	0.044	0.094	0.061	0.077
R^2	0.97	0.96	0.95	0.75	0.96	0.95
Pseudo second-order kinetic model						
q_e (mgg^{-1})	1.93	1.94	2.32	2.13	1.84	2.00
k_2 ($g\ mg^{-1}\ min^{-1}$)	0.18	0.17	0.28	0.60	0.31	0.14
R^2	0.99	0.98	0.99	0.99	0.99	0.99
Intraparticle diffusion						
First step						
k_i (mg g^{-1} $min^{-0.5}$)	0.213	0.447	0.230	0.237	0.430	0.369
C($mg\ g^{-1}$)	0.76	1.40	1.20	0.80	0.18	0.37
R^2	0.97	0.99	0.91	0.95	0.90	0.91
Second step						
k_i (mg g^{-1} $min^{-0.5}$)	0.183	0.229	0.124	0.173	0.073	0.080
C(mgg^{-1})	0.82	0.59	1.42	1.35	1.36	1.41
R^2	0.99	0.99	0.92	0.91	0.95	0.90

3.5. Evaluating thermodynamic parameters of sorption

Thermodynamic investigation sheds light on the feasibility and spontaneity of the sorption processes (Kundu and Gupta, 2006; Naseri et al., 2023). We compute thermodynamic parameters by using the following mathematical relations (Lima et al., 2019):

$$\Delta G^{\circ} = -RTlnK_e^0 \tag{14}$$

$$ln\ K_e^0 = -\frac{\Delta H^{\circ}}{R} \times \frac{1}{T} + \frac{\Delta S^{\circ}}{R} \tag{15}$$

$$K_e^0 = K_L \times 1000 \times MW_{Phosphate} \times C^{\circ} \tag{16}$$

By plotting Ln K against T^{-1} (Fig. 15), we computed the values of ΔH and ΔS from the intercepts and slopes. Using this approach, we calculated the enthalpy change (ΔH), free energy change (ΔG), and entropy change (ΔS) for the adsorbent-adsorbate system (Table 7). Here, K is the equilibrium thermodynamic constant (dimensionless), ΔH°, ΔS°, and ΔG° represent changes in standard enthalpy, standard entropy, and standard free energy of adsorption, respectively. MW Phosphate is the

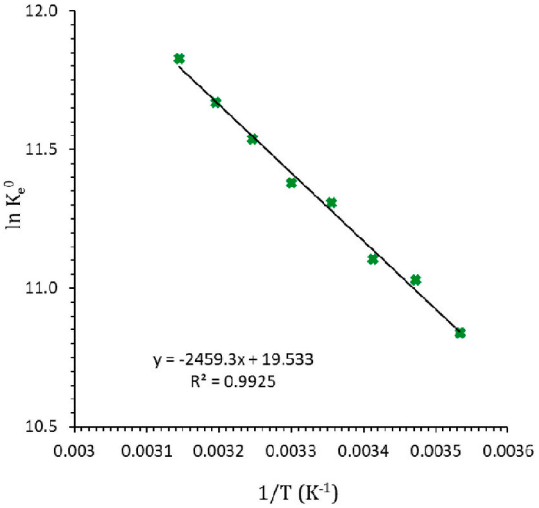


Fig. 15. Evolution of $ln\ K_e^0$ vs $1/T$.

Table 7
Values of the thermodynamic parameters.

T(K)	ΔH^0(kJ.mol^{-1})	ΔS^0(J.mol^{-1}. K^{-1})	-ΔG^0(kJ.mol^{-1})
283	22.902	184.380	25.503
288			26.415
293			27.051
298			28.017
303			28.663
308			29.546
313			30.364
318			31.273

molecular weight of phosphate, C° is the standard concentration (1 mol L^{-1}), and R is the gas constant (8.314 JK^{-1}mol^{-1}).

The ΔG° values were negative for the tested temperatures, indicating the spontaneity and favorability of the sorption process. Smith and Van Ness (1987) noted that low values of ΔG° are consistent with electrostatic interactions between sorption sites and sorbing ions (physical adsorptions) (Smith and Van Ness, 1987). According to Erdoğan et al. (2017), a positive value of ΔH° confirms the endothermic nature of sorption. Additionally, the positive value of ΔS° (standard entropy change) indicates an increase in the degree of freedom (or disorder) of the sorbed species (Das et al., 2006). The magnitude of enthalpy changes (ΔH°) between 2.1 to 21.0 and 80.0–200.0 kJ mol^{-1} suggests physisorption and chemisorption, respectively (Kundu and Gupta, 2006). Thus, the positive value of ΔH° of 22.902 indicates that phosphate uptake from the aqueous phase proceeds via some physiochemical interactions (Hu et al., 2023), suggesting that electrostatic attraction and complexation along with ion exchange have major roles in the uptake process.

3.6. Comparing SEM and EDS before and after adsorption

SEM imaging conducted after phosphate adsorption on Alum sludge revealed flocs on the surface (Fig. 16). These flocs may result from condensing small particles on the Alum sludge surface.

EDS analysis confirmed the presence of phosphorus on the Alum sludge surface (Fig. 17), suggesting that phosphorus has indeed attached to the Alum sludge surface. Consequently, Alum sludge has been demonstrated to remove phosphate from aqueous solutions.

3.7. Mechanisms of phosphate removal by alum sludge

Different mechanisms such as ion exchange, adsorption and complexation have been proposed to explain the removal of phosphate from aqueous solutions. The pH of the solution plays a critical role in the rate and mechanism of the removal of phosphate.

The possible adsorption mechanism for the removal of phosphate could be an adsorption process through the ion exchange between phosphate and hydroxide groups on the surface of Alum sludge (Lu et al., 2009). In addition, the presence of Al, Fe and Ca in alum sludge promotes complexation between phosphate anions and these cations. The ligand exchange and complexation of phosphorus with Fe, Al, and Ca ions were reported as main mechanism for removal of phosphorus by sludge based adsorbents (Devi and Saroha, 2017). As mentioned in section 3.5, the magnitude of enthalpy changes (22.902) indicates that phosphate uptake from the aqueous phase proceeds via some physiochemical interactions (Long et al., 2011), suggesting that some mechanisms like complexation and electrostatic attraction along with ion exchange have major roles in the uptake process.

3.8. Application

To scrutinize the practical applicability of Alum sludge for phosphate removal from wastewaters, a real effluent was elected from dairy unit of Boudouaou situated in the East of Algiers. After filtration of wastewater, the pH, temperature and concentration of phosphate were determined.

The results highlight an important phosphate concentration of 13 mg.L^{-1}. Then, it turns out that this concentration is beyond permissible level of phosphate discharge in wastwater (2 mg L^{-1}). As a result, wastwater has to be treated in order to limit the phosphate concentration and have to acceptable levels before it is released into the environments. The pH and temperature values agree with legal limits.

The application was made under the optimum conditions found during this study. The effectiveness of treatment was followed by the phosphate ions removal (Fig. 18). 88% of phosphate removal was achieved after 60 min of contact time, corresponding to 1.6 mg L^{-1}, less than the value of 2 mg L^{-1}, maximum allowable for wastewater discharge standard.

4. Conclusion

The results suggest that Alum sludge can serve as an effective and cost-efficient option for removing phosphate from aqueous systems. Its composition, including aluminium, iron, and calcium, grants it absorbent properties. In the batch experiments, optimal phosphate removal was achieved under specific conditions.: initial concentration (C0 = 100 mg L^{-1}), absorbent dosage (Cs = 20 g L^{-1}), pH (5), temperature (T = 23 °C), and stirring speed (N = 200 rpm). The kinetics of the process were rapid, reaching equilibrium within 60 min. The pH of the solutions notably influenced the removal of phosphate. Langmuir and pseudo-second-order models provided suitable fits for the phosphate sorption isotherm and kinetics, respectively. Thermodynamic analysis indicated that the sorption process was spontaneous, endothermic, and primarily physical. Applying optimal parameters to a dairy effluent resulted in a residual phosphate concentration meeting the discharge standard.

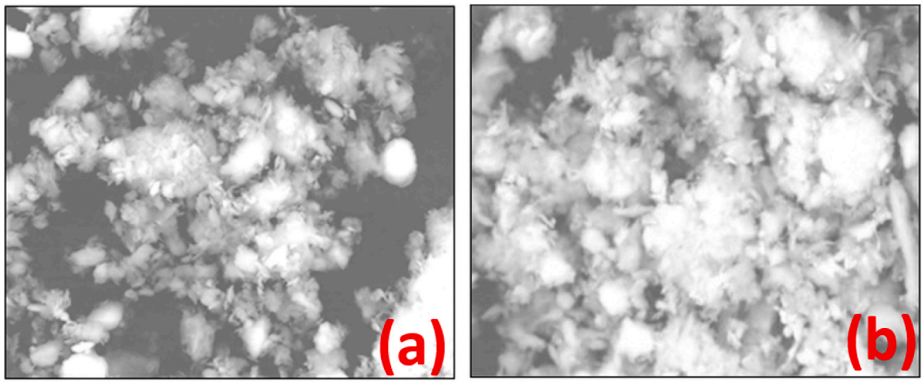


Fig. 16. SEM micrograph of Alum sludge before (a) and after adsorption (b).

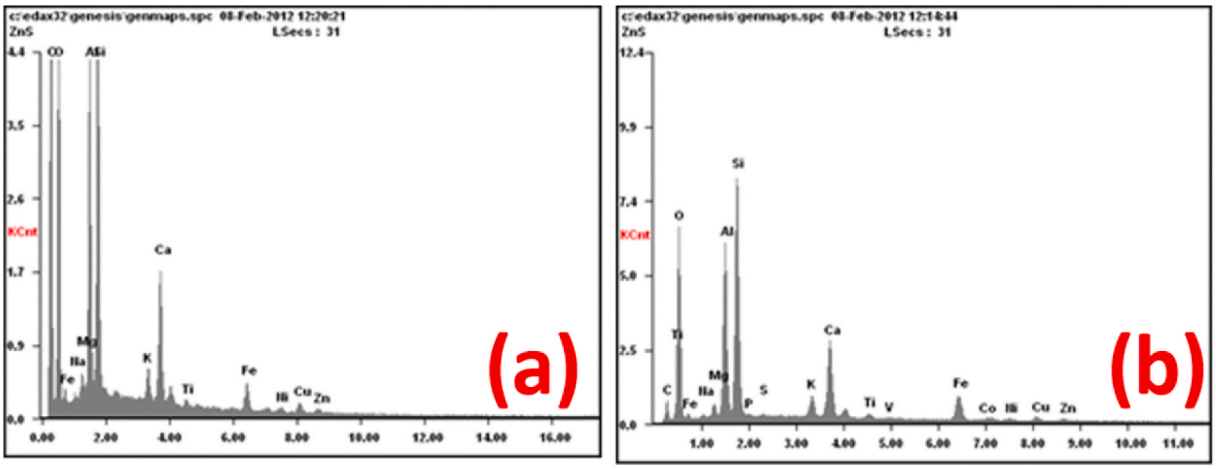


Fig. 17. Alum sludge EDS before (a) and after adsorption (b).

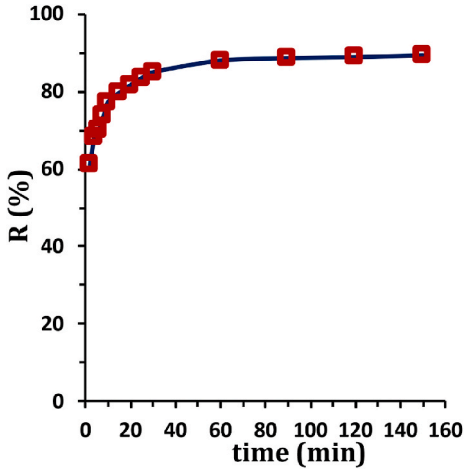


Fig. 18. Phosphate removal of the dairy industrial effluent.

Ethical approval

Not applicable.

Funding

Not applicable.

Nomenclature (list of symbols)

A_T	Tempkin constant	$(L.mg^{-1})$
b_T	Tempkin isotherm constant	
E	Mean free energy ($E = 1/\sqrt{2K_d}$)	$(kJ\ mol^{-1})$
B.E.T	Brunnauer, Emmet and Teller	
B	Constant relative to sorption heat	$(B = RT/b_T)\ (J.mol^{-1})$
C_0	Initial phosphate concentrations	$(mg.L^{-1})$
C_e	Phosphate concentrations at equilibrium	$(mg.L^{-1})$
C_s	Alum sludge concentrations in aqueous phase	$(g.L^{-1})$
C_t	Phosphate concentrations at 't' times	$(mg.L^{-1})$
K_L	Langmuir constant	$(L.mg^{-1})$
k_F	Freundlich isotherm constant	$(L.g^{-1})$
K_d	Dubinin–Radushkevich isotherm constant	$(mol^2\ kJ^{-2})$
ε	Dubinin–Radushkevich isotherm constant	$(\varepsilon = RT \ln [1+(1/C_e)])$
k_1	Rate constant for a pseudo-first order model	(s^{-1})
k_2	Rate constant for the pseudo second-order model	(s^{-1})
m	Mass of alum sludge	(mg)
n	Sorption intensity	

(*continued on next column*)

(*continued*)

q_e	Sorption capacity at equilibrium	$(mg.g^{-1})$
q_m	Maximal capacity of sorption	$(mg.g^{-1})$
q_t	Sorption capacity at 't' times	$(mg.g^{-1})$
R	Gases universal constant (8.314)	$(J.mol^{-1}.K^{-1})$
R^2	Coefficients of correlation	
T	Temperatures	(Kelvin)
V	Volumes of solution	(mL)
N	Stirring rates	(rpm)
ΔH°	Standard enthalpy change	$(KJ.mol^{-1})$
ΔS°	Standard entropy change	$(KJ.mol^{-1}.K^{-1})$
ΔG°	Standard free enthalpy change	$(KJ.mol^{-1})$
K_e^0	Thermodynamic equilibrium constant	–

CRediT authorship contribution statement

Leila Djekoune: Data curation, Investigation, Writing – original draft, Writing – review & editing. **Aziz Maaliou:** Writing – original draft, Writing – review & editing. **Zineb Salem:** Conceptualization, Funding acquisition. **Dalila Ziani:** Data curation, Investigation. **Raouf Kamel:** Data curation, Investigation. **Abdelkader Ouakouak:** Conceptualization, Writing – review & editing. **Omirserik Baigenzhenov:** Software, Writing – review & editing. **Dmitry Olegovich Bokov:** Software, Writing – review & editing. **Andrei Ivanets:** Software, Writing – review & editing. **Ahmad Hosseini-Bandegharaei:** Conceptualization, Software, Writing – review & editing.

Declaration of competing interest

The authors declare that they have no known competing financial interests or personal relationships that could have appeared to influence the work reported in this paper.

Data availability

Data will be made available on request.

References

Abo-El-Enein, S., Shebl, A., El-Dahab, S.A., 2017. Drinking water treatment sludge as an efficient adsorbent for heavy metals removal. Appl. Clay Sci. 146, 343–349.

Adhikari, R.A., Bal Krishna, K., Sarukkalige, R., 2016. Evaluation of phosphorus adsorption capacity of various filter materials from aqueous solution. Adsorpt. Sci. Technol. 34 (4–5), 320–330.

Babatunde, A., Zhao, Y., Zhao, X., 2010. Alum sludge-based constructed wetland system for enhanced removal of P and OM from wastewater: concept, design and performance analysis. Bioresour. Technol. 101 (16), 6576–6579.

Bulut, E., Ozacar, M., Sengil, I.A., 2008. Equilibrium and kinetic data and process design for adsorption of Congo Red onto bentonite. J. Hazard Mater. 154, 613–622.

Chen, T.C., Shih, Y.J., Chang, C.C., Huang, Y.H., 2013. Novel adsorbent of removal phosphate from TFT LCD wastewater. J. Taiwan Inst. Chem. Eng. 44, 61–66.
Cheng, X., Huang, X., Wang, X., Sun, D., 2010. Influence of calcination on the adsorptive removal of phosphate by Zn–Al layered double hydroxides from excess sludge liquor. J. Hazard Mater. 177, 516–523.
Chu, W., 2001. Dye removal from textile dye wastewater using recycled alum sludge. Water Res. 35 (13), 3147–3152.
Das, J., Patra, B., Baliarsingh, N., Parida, K., 2006. Adsorption of phosphate by layered double hydroxides in aqueous solutions. Appl. Clay Sci. 32 (3–4), 252–260.
Devi, P., Saroha, A.K., 2017. Utilization of sludge based adsorbents for the removal of various pollutants: a review. Sci. Total Environ. 578, 16–33.
Djekoune, L., Salem, Z., Maaliou, A., Boucetta, S., Ouakouak, A., 2022. Reuse of sludge from drinking water production in dye wastewater treatment of textile industry. Desalination Water Treat. 277, 72–84.
Erdoğan, S., Akmil Başar, C., Önal, Y., 2017. Particle size effect of raw material on the pore structure of carbon support and its adsorption capability. Part. Sci. Technol. 35 (3), 330–337.
Foo, K.Y., Hameed, B.H., 2010. Insights into the modeling of adsorption isotherm systems. Chem. Eng. J. 156 (1), 2–10.
Fragoso, R., Duarte, E., 2012. Reuse of drinking water treatment sludge for olive oil mill wastewater treatment. Water Sci. Technol. 66 (4), 887–894.
Ge, S., Zhang, H., Ye, H., Zhang, H., Zhao, K., Sun, Q., Cao, W., 2013a. Sorption behavior of phosphate on an MSWI bottom slag and sewage sludge co-sintered adsorbent. Water Air Soil Pollut. 224, 1–11.
Ge, S., Zhang, H., Ye, H., Zhang, H., Zhao, K., Sun, Q., Cao, W., 2013b. Sorption behavior of phosphate on an MSWI bottom slag and sewage sludge co-sintered adsorbent. Water Air Soil Pollut. 224, 1–11.
Harrison, R.M., 2001. Pollution: Causes, Effects and Control. Royal Society of Chemistry, London, UK.
Hu, X.J., Wang, J.S., Liu, Y.G., Li, X., Zeng, G.M., Bao, Z.L., Zeng, X.X., Chen, A.W., Long, F., 2011. Adsorption of chromium (VI) by ethylenediamine-modified crosslinked magnetic chitosan resin: isotherms, kinetics and thermodynamics. J. Hazard Mater. 185, 306–314.
Hu, Q.-D., Jiang, H.-L., Lam, K.-H., Hu, Z.-P., Liu, Z.-J., Wang, H.-Y., et al., 2023. Polydopamine-modification of a magnetic composite constructed from citric acid–cross-linked cyclodextrin and graphene oxide for dye removal from waters. Environ. Sci. Pollut. Control Ser. 2023, 1–16 (in press).
Jeon, E.-K., Ryu, S., Park, S.-W., Wang, L., Tsang, D.C., Baek, K., 2018. Enhanced adsorption of arsenic onto alum sludge modified by calcination. J. Clean. Prod. 176, 54–62.
Khitous, M., Salem, Z., Halliche, D., 2016a. Removal of phosphate from industrial wastewater using uncalcined MgAl-NO3 layered double hydroxide: batch study and modeling. Desalination Water Treat. 57 (34), 15920–15931.
Khitous, M., Salem, Z., Halliche, D., 2016b. Removal of phosphate from industrial wastewater using uncalcined MgAl-NO3 layered double hydroxide: batch study and modeling. Desalination Water Treat. 57 (34), 15920–15931.
Kundu, S., Gupta, A.K., 2006. Arsenic adsorption onto iron oxide-coated cement (IOCC): regression analysis of equilibrium data with several isotherm models and their optimization. Chem. Eng. J. 122 (1–2), 93–106.
Langmuir, I., 1916. The constitution and fundamental properties of solids and liquids. Part I. Solids. J. Am. Chem. Soc. 38 (11), 2221–2295.
Lee, C.-G., Park, J.-A., Kim, S.-B., 2012. Phosphate removal from aqueous solutions using slag microspheres. Desalination Water Treat. 44 (1–3), 229–236.
Li, G., Chen, D., Zhao, W., Zhang, X., 2015. Efficient adsorption behavior of phosphate on La-modified tourmaline. J. Environ. Chem. Eng. 3 (1), 515–522, 2015.
Li, C., Yu, Y., Li, Q., Zhong, H., Wang, S., 2019. Kinetics and equilibrium studies of phosphate removal from aqueous solution by calcium silicate hydrate synthesized from electrolytic manganese residue. Adsorpt. Sci. Technol. 37 (7–8), 547–565.
Lima, E.C., Hosseini-Bandegharaei, A., Moreno-Piraján, J.C., Anastopoulos, I., 2019. A critical review of the estimation of the thermodynamic parameters on adsorption equilibria. Wrong use of equilibrium constant in the Van't Hoof equation for calculation of thermodynamic parameters of adsorption. J. Mol. Liq. 273, 425–434.
Long, F., Gong, J.-L., Zeng, G.-M., Chen, L., Wang, X.-Y., Deng, J.-H., et al., 2011. Removal of phosphate from aqueous solution by magnetic Fe–Zr binary oxide. Chem. Eng. J. 171 (2), 448–455.
Lu, S., Bai, S., Zhu, L., Shan, H., 2009. Removal mechanism of phosphate from aqueous solution by fly ash. J. Hazard Mater. 161 (1), 95–101.
Lǔ, J., Liu, H., Liu, R., Zhao, X., Sun, L., Qu, J., 2013. Adsorptive removal of phosphate by a nanostructured Fe–Al–Mn trimetal oxide adsorbent. Powder Technol. 233, 146–154.
Makris, K.C., Sarkar, D., Datta, R., 2006. Evaluating a drinking-water waste by-product as a novel sorbent for arsenic. Chemosphere 64 (5), 730–741.
Mangwandi, C., Albadarin, A.B., Glocheux, Y., Walker, G.M., 2014. Removal of ortho-phosphate from aqueous solution by adsorption onto dolomite. J. Environ. Chem. Eng. 2 (2), 1123–1130.
Mohammed, W.T., Rashid, S.A., 2012. Phosphorus removal from wastewater using oven-dried alum sludge. Int. J. Chem. Eng. 2012, 1–11. Articale ID 125296.
Moharami S, Jalali M. Removal of phosphorus from aqueous solution by Iranian natural adsorbents. Chem. Eng. J. 223:328-339.
Moreira, R.F., Vandresen, S., Luiz, D.B., José, H.J., Puma, G.L., 2017. Adsorption of arsenate, phosphate and humic acids onto acicular goethite nanoparticles recovered from acid mine drainage. J. Environ. Chem. Eng. 5 (1), 652–659.
Naseri, A., Abed, Z., Rajabi, M., Asghari, A., Lal, B., Baigenzhenov, O., et al., 2023. Use of Chrysosporium/carbon nanotubes for preconcentration of ultra-trace cadmium levels from various samples after extensive studies on its adsorption properties. Chemosphere 335, 139168.
Nassef, E., 2012. Removal of phosphates from industrial waste water by chemical precipitation. Engineering Science and Technology: Int. J. 2 (3), 409–413.
Nthumbi, R.M., Ngila, J.C., Moodley, B., Kindness, A., Petrik, L., 2012. Application of chitosan/polyacrylamide nanofibres for removal of chromate and phosphate in water. Phys. Chem. Earth, Parts A/B/C 50, 243–251.
Peiravi-Rivash, O., Mashreghi, M., Baigenzhenov, O., Hosseini-Bandegharaei, A., 2023. Producing bacterial nano-cellulose and keratin from wastes to synthesize keratin/cellulose nanobiocomposite for removal of dyes and heavy metal ions from waters and wastewaters. Colloids Surf. A Physicochem. Eng. Asp. 656, 130355.
Piaskowski, K., 2013. Orthophosphate removal from aqueous solutions using drinking-water treatment sludge. Water Sci. Technol. 68 (8), 1757–1762.
Qasemi, M., Hosseini-Bandegharaei, A., Afsharnia, M., Najafpoor, A., Ivanets, A., López-Delgado, A., et al., 2018. Thermally treated aluminium waste-filings, a low cost and efficient adsorbent for phosphorus removal from water. Global NEST Journal 20 (3), 488–496.
Sirajo, L., Zaini, M.A.A., 2023. Iron-loaded coconut shell-activated carbons for orthophosphate adsorption. Biomass Conversion and Biorefinery 1–14 (in press).
Siswoyo, E., Mihara, Y., Tanaka, S., 2014. Determination of key components and adsorption capacity of a low cost adsorbent based on sludge of drinking water treatment plant to adsorb cadmium ion in water. Appl. Clay Sci. 97, 146–152.
Smith, J.M., Van Ness, H.C., 1987. Introduction to Chemical Engineering Thermodynamics, fourth ed. McGraw-Hill, Singapore.
Sotero-Santos, R.B., Rocha, O., Povinelli, J., 2005. Evaluation of water treatment sludges toxicity using the Daphnia bioassay. Water Res. 39 (16), 3909–3917.
Sujana, M., Thakur, R., Rao, S., 1998. Removal of fluoride from aqueous solution by using alum sludge. J. Colloid Interface Sci. 206 (1), 94–101.
Sun, Q., Yang, L., 2003. The adsorption of basic dyes from aqueous solution on modified peat–resin particle. Water Res. 37 (7), 1535–1544.
Tang, Y., Tong, Z., Wei, G., 2006. Removal of phosphate from aqueous solution with modified bentonite. Chin. J. Process Eng. 6 (2), 197–200.
Xiong, J., Qin, Y., Islam, E., Yue, M., Wang, W., 2011. Phosphate removal from solution using powdered freshwater mussel shells. Desalination 276, 317–321.
Xu, K., Deng, T., Liu, J., Peng, W., 2012a. Phosphate removal from digested sludge supernatant using modified fly ash. Water Environ. Res. 84 (5), 411–416.
Xu, K., Deng, T., Liu, J., Peng, W., 2012b. Phosphate removal from digested sludge supernatant using modified fly ash. Water Environ. Res. 84 (5), 411–416.
Yan, Y., Sun, X., Ma, F., Li, J., Shen, J., Han, W., Liu, X., Wang, L., 2014. Removal of phosphate from wastewater using alkaline residue. J. Environ. Sci. 26, 970–980.
Yang, Y., Zhao, Y., Babatunde, A., Wang, L., Ren, Y., Han, Y., 2006. Characteristics and mechanisms of phosphate adsorption on dewatered alum sludge. Separ. Purif. Technol. 51 (2), 193–200.
Yang, Y., Zhao, Y., Kearney, P., 2008. Influence of ageing on the structure and phosphate adsorption capacity of dewatered alum sludge. Chem. Eng. J. 145 (2), 276–284.
Ye, H., Chen, F., Sheng, Y., Sheng, G., Fu, J., 2006. Adsorption of phosphate from aqueous solution onto modified palygorskites. Separ. Purif. Technol. 50 (3), 283–290.
Yeddou Mezenner, N., Bensmaili, A., 2009. Kinetics and thermodynamic study of phosphate adsorption on iron hydroxide-eggshell waste. Chem. Eng. J. 147, 87–96.
Yousif, A.M., Rodgers, M., Clifford, E., 2012. Studying the adsorption properties of modified red mud towards phosphate removal from its solutions. Int. J. Environ. Sustain Dev. 3 (4), 354–356.
Yue, Q., Zhao, Y., Li, Q., Li, W., Gao, B., Han, S., et al., 2013. Research on the characteristics of red mud granular adsorbents (RMGA) for phosphate removal. J. Hazard Mater. 176 (1–3), 741–748, 2010.
Zhang, B., Wu, D., Wang, C., He, S., 2007. Simultaneous removal of ammonium and phosphate by zeolite synthesized from coal fly ash as influenced by acid treatment. J. Environ. Sci. 19, 540–545.
Zhang, J., Shen, Z., Shan, W., Chen, Z., Mei, Z., Lei, Y., et al., 2010a. Adsorption behavior of phosphate on Lanthanum (III) doped mesoporous silicates material. J. Environ. Sci. 22 (4), 507–511.
Zhang, J., Shen, Z., Shan, W., Chen, Z., Mei, Z., Lei, Y., et al., 2010b. Adsorption behavior of phosphate on Lanthanum (III) doped mesoporous silicates material. J. Environ. Sci. 22 (4), 507–511.
Zhao, Y., Yue, Q., Li, Q., Xu, X., Yang, Z., Wang, X., et al., 2012a. Characterization of red mud granular adsorbent (RMGA) and its performance on phosphate removal from aqueous solution. Chem. Eng. J. 193, 161–168.
Zhao, Y., Yue, Q., Li, Q., Xu, X., Yang, Z., Wang, X., et al., 2012b. Characterization of red mud granular adsorbent (RMGA) and its performance on phosphate removal from aqueous solution. Chem. Eng. J. 193, 161–168.
Zhu, Y., Yue, X., Xie, F., 2020. Adsorptive removal of phosphate by a Fe–Mn–La tri-metal composite sorbent: adsorption capacity, influence factors, and mechanism. Adsorpt. Sci. Technol. 38 (7–8), 254–270.